STRUCTURE NONLINEARITY AND RESPONSE OF LATERALLY LOADED PILES

Wei Dong Guo[1] **and B. T. Zhu**[2]
[1]*School of Civil, Mining & Environmental, Engineering, University of Wollongong*
[2]*Arup Pty Ltd, Level 4 108 Wickham Street, Fortitude Valley, Qld, 4006*

ABSTRACT

In light of a generic limiting force profile (LFP), closed-form solutions for laterally loaded free- and fixed- head piles in elastic-plastic media have been developed, and implemented by the first author into a spreadsheet program called GASLFP. The solutions offer an expeditious and sufficiently accurate prediction of response of lateral piles. Conversely, they allow input parameters to be deduced using measured pile response, as has been conducted for over 70 test (elastic) piles to date. Nevertheless, structure nonlinearity of pile body is an important issue at a large deflection.

In this paper, a semi-empirical approach is established to capture pile response owing to structural nonlinearity. Expressions were provided for gaining cracking moment M_{cr}, flexural rigidity of cracked cross section E_pI_p, and ultimate bending moment M_{ult}. Against measured response of two laterally loaded single piles, back-estimation indicates that (1) the parameters for elastic piles are quite consistent with the previous findings for piles in sand and clay, (2) The proposed variations of M_{cr}, E_pI_p and M_{ult} for nonlinear piles provide good prediction of the pile response against measured data and (3) the modulus of rupture k_r of 16.7 (clay) and 33.0(sand) are close to those adopted for structural beams, although a very high k_r of 62.7 (thus resulting in higher M_{cr}) for a pile in sand was deduced (shown elsewhere). The use of the k_r for beams would render pile deflections of the later pile to be significantly overestimated. The conclusions may be incorporated into design of laterally loaded piles.

1 INTRODUCTION

A number of approaches based on p-y concept were developed to capture the behaviour of piles subjected to lateral loads (McClelland and Focht 1958; Matlock 1970; Reese *et al.,* 1974; Reese *et al.*, 1975). The behaviour is generally dominated by the limiting force per unit length p_u mobilized between the pile and soil, especially at high load levels (Randolph *et al.*,1988; Guo 2006). The profile of p_u (also referred to as LFP) along the pile may be constructed using empirical or semi-empirical methods proposed previously (Brinch Hansen 1961; Broms 1964; Matlock 1970; Reese *et al,.* 1974; Reese *et al.,* 1975; Barton 1982; Guo 2006). In light of a generic LFP, elastic-plastic, closed-form (CF) solutions were developed for laterally loaded free- and fixed- head piles (Guo 2006; Guo 2009), respectively. The solutions allow pile response to be predicted in an effective and efficient manner. Conversely, they enable the LFP to be deduced against measured pile response. They, however, are limited to elastic piles, and structure nonlinearity of pile body is an important issue at a large deflection (Nakai and Kishida 1982; Reese 1997; Huang *et al*., 2001; Ng *et al*., 2001; Zhang 2003).

2 SOLUTIONS FOR LATERALLY LOADED PILES

The problem of a laterally loaded free-head pile is schematically shown in Figure 1(a), with a lateral load P_t applied at an eccentricity, e above ground level (GL). The pile-head is free to rotate and translate with no constraint imposed at the pile head and along the effective pile length except for soil resistance. The pile-soil interaction is captured by a physical spring-slider model presented in Figure 1(b) with the lateral load P_t and a moment, M_t (= P_te) applied at the GL. The pile is described by deflection y (along the pile axis) at a depth x (below the origin at the GL). The interaction at each depth is modelled by a spring in series with a slider characterized by an idealized elastic-plastic p-y curve (see Figure 1c). The spring has a subgrade modulus, k (i.e. the slope of the p-y curve), and the slider provides a limiting force per unit length p_u for the pile-soil interaction. The soil resistance normally reaches the p_u (varying with depth) over a depth called slip depth, x_p that increases with loading. Above the depth x_p, the pile-soil interaction is in plastic state; whereas below the x_p, it is in elastic state. The elastic state is modelled by the independent springs linked by a fictitious membrane with a constant fictitious tension, N_p (i.e. incorporating the coupled effect among springs via a coupled load transfer model). In the plastic zone, however, the tension is neglected by taking N_p as zero (employing an uncoupled load transfer model).

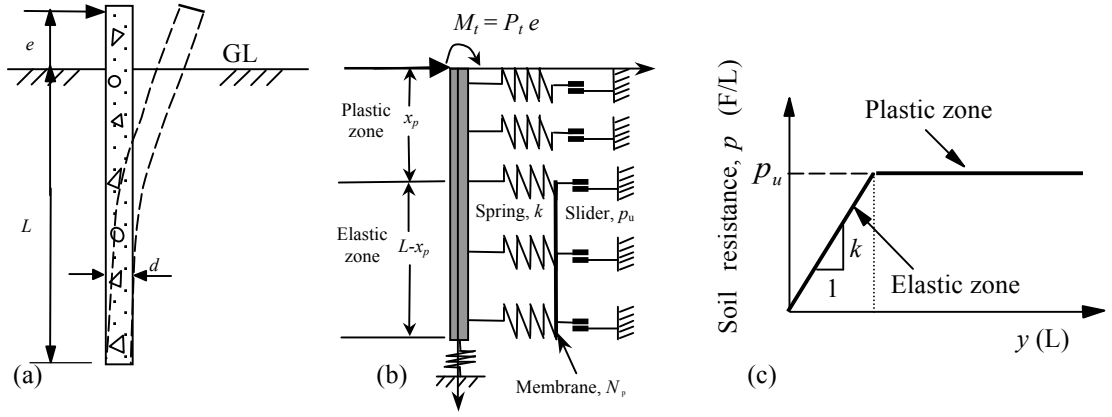

Figure 1: Coupled load transfer analysis for a free-head pile (Guo, 2001a, 2006): (a) The problem addressed, (b) Coupled load transfer model and (c) Load transfer (p-y) curve.

In the elastic state ($x<x_p$), the subgrade modulus k and the fictitious tension, N_p are obtained previously (Guo and Lee 2001). As shown in Table 1, they are mainly functions of Young's modulus of an equivalent solid pile, E_p [$=E_pI_p/(\pi d^4/64)$] and an equivalent soil shear modulus G^* [$=(1+0.75\nu_s)G_s$], in which E_pI_p and d = flexural rigidity, and outside diameter of the pile, respectively; ν_s and G_s = Poisson's ratio and shear modulus of soil, respectively. In the plastic zone ($x \geq x_p$), the limiting force per unit length p_u is well captured by (Guo 2001a)

$$p_u = A_L(\alpha_o + x)^n \qquad (1)$$

where p_u = limiting force per unit length [FL^{-1}]; $A_L = s_u N_g d^{1-n}$ (clay), and $\gamma_s' N_g d^{2-n}$ (sand), gradient of the LFP [FL^{-1-n}]; α_o = a constant to include the force at the GL [L]; x = depth below the GL [L]; n = a power to the sum of α_o and x; N_g = limiting force factor; s_u = undrained shear strength of cohesive soil [FL^{-2}]; and γ_s' = effect unit weight of the soil [FL^{-3}]. Guo (2006) shows

- $G_s = (0.25\sim0.62)N$ (MPa) ($\overline{G}_s = 0.5N$ MPa, note the bar denotes average and N = blow counts of SPT), $\alpha_o = 0$, $n = 1.7$ and $N_g = (0.4\sim2.5)K_p^2$ with respect to a uniform sand profile in which $K_p = \tan^2(45^o + \phi_s/2)$; and ϕ_s = effective friction angle of the soil
- $G_s = (25\sim315)s_u$ ($\overline{G}_s = 92.3s_u$), $n = 0.7$, $\alpha_o = 0.05\sim0.2$ m ($\overline{\alpha}_o = 0.11$m), and $N_g = 0.6\sim3.2$ ($\overline{N}_g = 1.6$) for a uniform clay profile.
- The construction of LFP and use of an average G_s for layered soil profiles.

The LFP described by Eq. (1) will be referred to as *Guo* LFP. It is provided in Table 1 along with Reese LFP for cohesionless soil, Matlock LFP for cohesive soil and Hansen LFP for any subsoil (using cohesion c and ϕ_s).

The pile-soil interaction is governed by two differential equations that are dominated by the p_u in the plastic zone ($0 \leq x \leq x_p$) and by the k and N_p in elastic zone, respectively. They were resolved using boundary conditions and presented in closed-form expressions for pile deflection, slope, bending moment, shear force and soil resistance. The expressions are featured by reciprocal of characteristic length of the pile λ ($= [k/(4E_pI_p)]^{0.25}$ with k/G_s =2.4~3.92), the slip depth x_p and the parameters A_L (or N_g), α_o, and n (for the LFP). For instance, ignoring ground level resistance (by taking $\alpha_o = 0$) and using a uncoupled model ($N_p = 0$), the pile deflection at GL y_o is given by (Guo 2006)

$$\frac{y_o k\lambda^n}{A_L} = \frac{2}{3}\bar{x}_p^{n+3}\frac{2\bar{x}_p^2 + (2n+10)\bar{x}_p + n^2 + 9n + 20}{(\bar{x}_p + 1 + \bar{e})(n+2)(n+4)} + \frac{(2\bar{x}_p^2 + 2\bar{x}_p + 1)\bar{x}_p^n}{\bar{x}_p + 1 + \bar{e}} + \frac{2\bar{x}_p^4 + (n+4)(\bar{x}_p + 1)[2\bar{x}_p^2 + (n+1)(\bar{x}_p + 1)]}{(\bar{x}_p + 1 + \bar{e})(n+1)(n+4)}\bar{e}\bar{x}_p^n + \frac{4}{3}\bar{P}_t\bar{e}^3 \qquad (2)$$

where $\bar{x}_p = \lambda x_p, \bar{e} = \lambda e$, and $\bar{P}_t = P_t\lambda^{1+n}/A_L$. The solutions were entered into a spreadsheet program GASLFP. The solutions well captures the response of laterally loaded piles. Conversely, they allows the values of A_L (or N_g), α_o, *n, and* G_s to be deduced by matching the predicted with measured pile response of maximum bending moment (M_{max}), pile deflection y_o, and so forth under each load P_t. The solutions are developed for a

pile with a length L exceeding the critical value L_{cr} [= $1.05d(E_p/G_s)^{0.25}$], beyond which any extra length of a pile will impose negligible influence on the pile response; otherwise the solutions for short rigid piles (Guo 2008) should be adopted. Note the G_s may be taken as the average $\overline{G}_s$ over a depth of 10*d*. GASLFP is used to conduct current investigation.

Table 1 Typical limiting force profiles

Name	Expressions
Matlock LFP	$N_g = \gamma_s' d/\bar{s}_u + 0.5, \alpha_o = 2d/N_g,\ n = 1$ (Matlock 1970)
Reese LFP (sand) (Reese *et al*., 1974)	$p_u = \gamma_s' x\{f_{r1}x + [\frac{\tan\beta}{\tan(\beta-\phi_s)} - K_a]d\}$ ($x<x_t$) $p_u = \gamma_s' x[K_a d(\tan^8\beta - 1) + K_o \tan\phi_s \tan^4\beta]$ ($x\geq x_t$) $f_{r1} = \frac{\tan\beta}{\tan(\beta-\phi_s)}(\frac{K_o \tan\phi_s \cos\beta}{\cos\alpha} + \tan\beta\tan\alpha) + K_o \tan\beta(\tan\phi_s \sin\beta - \tan\alpha)$ K_o=1-*sin*ϕ_s,$\alpha = 0.5\phi_s$, β= *45+0.5*ϕ_s, K_a=*tan*^{2}(45-0.5ϕ_s), and x_t = critical depth. A modification of the calculated p_u is used
Hansen LFP (Hansen 1961)	$p_u = (K_q^D \gamma_s' x + K_c^D c)d$ where $K_q^D = (K_q^o + \alpha_q K_q^\infty \frac{x}{d})/(1+\alpha_q \frac{x}{d})$, $K_c^D = (K_c^o + \alpha_c K_c^\infty \frac{x}{d})/(1+\alpha_c \frac{x}{d})$, $\alpha_q = K_q^o K_o \sin(\phi_s)/[(K_q^\infty - K_q^o)\sin(45^o + 0.5\phi_s)]$, $\alpha_c = 2\sin(45^o + 0.5\phi_s)K_c^o/[(K_c^\infty - K_c^o)]$ $K_q^o = e^{(0.5\pi+\phi_s)\tan\phi_s}\cos\phi_s \tan(45^o + 0.5\phi_s) - e^{-(0.5\pi-\phi_s)\tan\phi_s}\cos\phi_s \tan(45^o - 0.5\phi_s)$, $K_c^o = [e^{(0.5\pi+\phi_s)\tan\phi_s}\cos\phi_s \tan(45^o + 0.5\phi_s) - 1]\mathrm{ctan}\phi_s$ $K_c^\infty = (1.58 + 4.09\tan^4\phi_s)[e^{\pi\tan\phi_s}\tan(45^o + 0.5\phi_s) - 1]\mathrm{ctan}\phi_s$ $K_q^\infty = K_c^\infty(1 - \sin\phi_s)\tan\phi_s$
Guo LFP or Eq. (1) (Guo 2006)	Clay: $A_L = \bar{s}_u N_g d^{1-n}$, with α_o = 0.05~0.2 (m), n = 0.7 for clay, 1.5 for stiff, and N_g = 2~4 Sand: $A_L = \gamma_s' N_g d^{2-n}$, with α_o = 0, n = 1.7, and $N_g = s_g K_p^2$, in which s_g = an integral factor to cater for all sorts of influence; and $K_p = \tan^2(45^o + \phi_s/2)$, the passive earth pressure coefficient.
Note	$\frac{k}{G} = \frac{3\pi}{2}\left\{2\gamma\frac{K_1(\gamma)}{K_0(\gamma)} - \gamma^2\left[\left(\frac{K_1(\gamma)}{K_0(\gamma)}\right)^2 - 1\right]\right\}$ and $\frac{4N_p}{\pi d^2 G} = [K_1(\gamma)/K_0(\gamma)]^2 - 1$ where $K_j(\gamma)$ is modified Bessel function of second kind of j^{th} order (j = 0, 1) (Guo and Lee 2001) . The factor γ is for $L > L_{cr}+x_p$ and given by $\gamma = k_1(E_p/G^*)^{-0.25}$; with k_1 = 1.0 for a lateral load (e = 0) applied at point O (sliding level), and k_1 = 2.0 for a pure moment. The governing equations were resolved (Guo 2001a; Guo 2006) for free-head case, and a pile length exceeding the sum of $L_{cr} + x_p$.

3 MODELLING STRUCTURE NONLINEARITY

3.1 CRACKING MOMENT MCR

Tensile strength is only a small fraction of compressive strength for a concrete pile. Tensile cracks may be developed at a large deflection, once the tensile stress at the extreme fibre arrives at the modulus of rupture f_r. Section analysis of a beam allows the modulus f_r to be correlated with cracking moment, M_{cr} (upon which cracks are initiated) by:

$$\boldsymbol{M_{cr} = \frac{f_r I_g}{y_r} = k_r \frac{\sqrt{f_c'} I_g}{y_r}} \qquad (3)$$

where k_r = 19.7~31.5 for a normal weight concrete beam (ACI. 1993), and 16.7~62.7 for lateral piles (shown elsewhere); y_r = distance from centroidal axis of gross section to extreme fibres in tension; I_g = moment of inertia of gross section about centroidal axis (neglecting reinforcements); f_c' = characteristic value of the compressive strength of concrete, in kPa. The f_c' and E_c may be empirically correlated by $E_c = 151{,}000(f_c')^{0.5}$ (kPa) (ACI. 1993).

3.2 VARIATION OF EFFECTIVE FLEXURAL RIGIDITY E_PI_P WITH M_{MAX}

Under a lateral load, cracks may be induced in a pile at the depth of M_{max} if the M_{max} exceeds the cracking moment M_{cr}, although other regions may be still intact. This will render the flexural rigidity of the pile E_pI_p reduce from the elastic E_cI_g (rewritten as EI) to a new effective bending rigidity E_cI_e (rewritten as E_pI_p) (ACI. 1993) until a final (minimum) cracked rigidity $(EI)_{cr}$ (= E_cI_{cr}). This variation may be expressed by

$$E_pI_p = \left(\frac{M_{cr}}{M_{\max}}\right)^3 EI + \left[1-\left(\frac{M_{cr}}{M_{\max}}\right)^3\right](EI)_{cr} \qquad (4)$$

Equation (4) is used to deduce Young's modulus of a pile, E_p [= $E_cI_e/(\pi d^4/64)$, or $E_cI_e/(bh^3/12)$] from E_pI_p of the entire pile, regardless of the position and scale of cracks. This should model the worst scenario as the cracks should generally be confined to a limited zone; otherwise much more complicated procedure is required (Chiou *et al*., 2009). More importantly, replacing E_p in the elastic-pile solutions with this new E_p, nonlinear pile response is readily captured using the same solutions for elastic piles.

3.3 M_{ULT} AND I_{CR} FOR RECTANGULAR AND CIRCULAR CROSS SECTIONS

The ultimate bending moment M_{ult} and I_{cr} may be obtained by bending theory via moment-curvature method that involves stress-strain relationships of concrete and reinforcement (Hsu 1993). For instance, Reese (1997) provided the M_{ult} and I_{cr} for closely-spaced-cracks using a Hognestaad parabolic stress-strain relationship for concrete and an elastic-perfectly plastic stress-strain relationship for steel. The cracks may initially be spaced at some distance and the concrete stress-strain relationship depends on strength, rate and duration of loading etc. A rational flexural theory for reinforced concrete is thus yet to be developed (Nilson *et al*., 2004). Pragmatically, limit state design underpinned by simplified rectangular stress block method (referred to as RSB hereafter) (Whitney 1937) has been widely adopted to calculate the M_{ult} and I_{cr} (BSI 1985; EC2 1992; ACI. 1993).

A pile may generally fail by crushing of the concrete in the outmost compression fibre as tension failure of steel rebar is rare. The compression failure may occur at a strain ε_{cu} of 0.0035 (BSI 1985; EC2 1992; Nilson *et al*., 2004), or 0.003 (ACI. 1993). The tension failure strain ε_{su} varies from 10 to 40% (Lui 1997), and was taken as 0.015 (Reese 1997). The accuracy of ε_{su} has limited impact on analysing lateral piles showing compressive failure.

Figure 2 shows typical cracked cross-sections, with four rows of rebars, and of a circular pile (Figure 2a), and a rectangular pile (Figure 2b), respectively. With a linear strain distribution (Figure 2c), the compressive stress in concrete is simplified as a rectangular stress block (Figure 2d) characterised by those highlighted in Table 2, including the intensity of the stress, σ_c, the depth a of the stress block, and the stress induced in a rebar in the i^{th} row, σ_{si} . The stresses allow axial force bending moment in either section to be gained as.

$$\int_A \sigma dA = P_{xc} + P_{xs} = P_x \qquad (5)$$

$$\int_A \sigma x_1 dA = M_c + M_s = M_n \qquad (6)$$

where A = area of cross-section excluding the concrete in tension; σ = normal stress in concrete (σ_c) or rebars (σ_{si}); $P_{xc} = \sigma_c A_c$, axial load taken by the concrete; A_c = area of concrete in compression; $P_{xs} = \sum \sigma_{si} A_{si}$, axial load shared by the rebars; A_{si} = total area of rebars in the i^{th} row; P_x = imposed axial load; x_1 = distance from neutral axis; M_c and M_s = moments about the neutral axis induced by normal stress in the concrete and rebars, respectively; and M_n = nominal or calculated ultimate moment. Generally, the values of P_{xc}, P_{xs} and M_s can be readily obtained. The M_c may be estimated using Equations (7) and (8) developed herein for a rectangular and a circular cross-section, respectively.

$$M_c = f_c'' ab(2c-a)/2 \qquad (7)$$

or

$$M_c = 2r^2 f_c'' \left\{\left[\frac{a}{3r}(2-\frac{a}{r}) + \frac{1}{2}(1-\frac{c}{r})(1-\frac{a}{r})\right]\sqrt{2ra-a^2} + \frac{r-c}{2}[\arcsin(\frac{r-a}{r}) - \frac{\pi}{2}]\right\} \qquad (8)$$

where b = width of a rectangular pile.

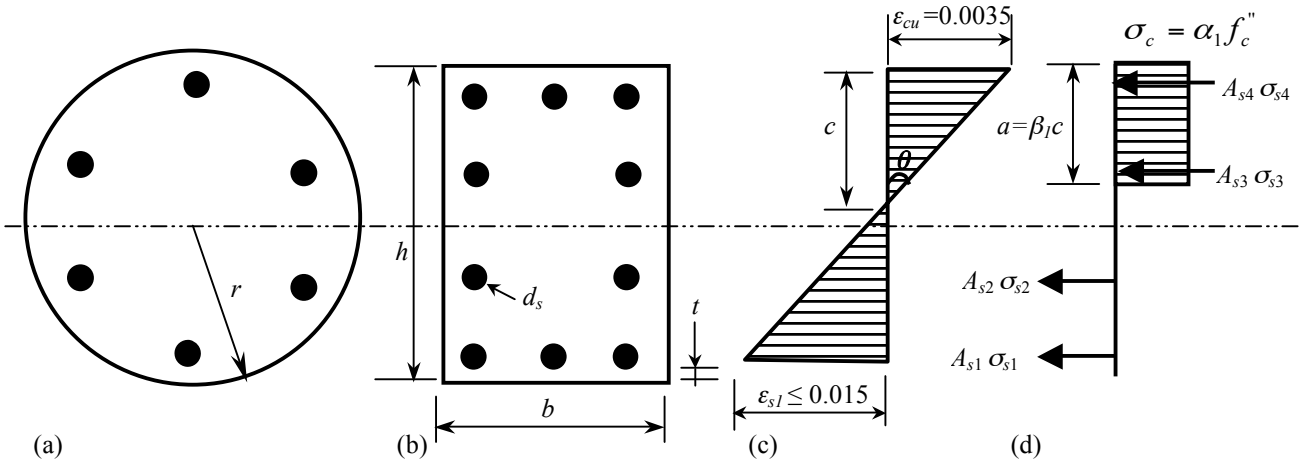

Note $f_c'' = 0.85 f_c'$; $\alpha_1 = 0.85$; $\beta_1 = 0.85\text{-}0.05(f_c'\text{-}27.6)/6.9$ and $\beta_1 \ge 0.65$; θ = curvature; t = cover thickness; $A_{s1}\ \sigma_{s1}$, $A_{s2}\ \sigma_{s2}$, $A_{s3}\ \sigma_{s3}$, $A_{s4}\ \sigma_{s4}$ are axial forces of the first to fourth row reinforcing bars and the rows are numbered consecutively from the extreme tensile bars to the compression side, in which σ_{si} = steel stress of a rebar in the ith row and A_{si} = total area of rebars in the i-th row.

Figure 2: Simplified rectangular stress block for ultimate bending moment calculation: a) Circular section, (b) Rectangular section (c) Strain, and (d) Stress.

Table 2 Stress block for calculating M_{ult}

Items	Description
σ_c	The intensity of the stress, σ_c is $\alpha_1 f_c''$ with $\alpha_1 = 0.85$, and $f_c'' = 0.85 f_c'$.
a	The depth a of the stress block is given by $a = \beta_1 c$, where $\beta_1 = 0.85\text{-}0.05(f_c'\text{-}27.6)/6.9$ and $\beta_1 \ge 0.65$, and c = distance from the outmost compression fibre to neutral axis: $c = 0.0035/\theta$ if concrete fails, otherwise $c = 2r - t - d_s/2 - 0.015/\theta$ concerning the debound (tension) failure. Note: The diameter of '2r' for a circular pile should be replaced with h for a rectangular pile; r = radius of a circular pile, θ = curvature at the limit state, d_s = diameter of rebars, and t = cover thickness (Fig. 2b).
σ_{si}	The stress induced in a rebar in i-th row, σ_{si} is calculated according to level of rebar strain ε_{si} (compared to yield strain ε_{sy}): $\sigma_{si} = \phi_r f_y$ (yield stress) if $\varepsilon_{si} > \varepsilon_{sy}$ otherwise, $\sigma_{si} = \varepsilon_{si} E_s$. Note: The ith row of rebars are counted from the farthest tensile row towards the compressive side (see Figure 2d); $\varepsilon_{sy} = \phi_r f_y / E_s$, E_s = Young's modulus of reinforcement, generally taken as 2×10^8 kPa; and ϕ_r=0.9, reinforcement reduction factor for tension and flexure.

Computing M_{ult} and I_{cr} may follow the steps highlighted in Table 3. First, the nominal ultimate bending moment M_n of $M_c + M_s$ is calculated using Equation (6); Second, the ultimate bending moment, M_{ult} is calculated as ϕM_n (ϕ = a reduction factor) (see Table 3); and finally the cracked flexural rigidity, $E_c I_{cr}$ is obtained by

$$E_c I_{cr} = M_{ult} / \theta \qquad (9)$$

The aforementioned calculation has been entered into a simple spreadsheet program that operates in EXCEL^{TM}. The program offers consistent results against the ACI, and the AS3600 methods (not shown herein), and was thus used in this study.

Table 3: Calculation of M_{max} and I_{cr} using RSB method

Steps	Actions
1	Select an initial curvature θ (see Figure 2) of $0.0035/r$;
2	Calculate position of neutral axis by evaluating c and $a = \beta_1 c$;
3	Compute the axial forces in concrete P_{xc} and rebars P_{xs};
4	Find squash load capacity P_{xu} by: $P_{xu} = f_c' A_c + E_s(f_c'/E_c)A_c$, where A_c, A_s = total areas of concrete and rebars, respectively;
5	If $P_{xc} + P_{xs} - P_{xu} > 10^{-4} P_{xu}$, increase θ by a designated increment, say $0.0035/1000r$. Otherwise, if $P_{xc} + P_{xs} - P_{xu} < -10^{-4} P_{xu}$, reduce the θ by the said amount. Repeat steps (1)~(4) until the convergence is achieved.
6	Estimate the nominal ultimate bending moment of $M_c + M_s$ by Eq. (6); and finally
7	Compute the ultimate bending moment, M_{ult} using $M_{ult} = \phi(M_c + M_s)$, in which ϕ = ultimate moment reduction factor, catering for difference between actual and nominal pile dimension, rebar cage off-position, and assumptions and simplifications inherent in the analysis. The ϕ is given by (Nilson *et al*., 2004) • $\phi = 0.493 + 83.3\varepsilon_{s1}$, and $0.65 \le \phi \le 0.9$, for laterally tied rebar cage; • $\phi = 0.567 + 66.7\varepsilon_{s1}$, and $0.70 \le \phi \le 0.9$, for spirally reinforced rebar cage.
8	Compute the cracked flexural rigidity, $E_c I_{cr}$ by $E_c I_{cr} = M_{ult}/\theta$
Notes	As an example, the calculations for the pile in sand are as follows: $\beta = 0.65$, $\theta = 0.0164$ (m^{-1}), c = 214 mm, $\varepsilon_{s1} = 0.00586$, a = 139 mm, P_{xc} = 2.8651MN, P_{xs}= -2.8654MN, M_c = 0.38 MNm, M_s = 1.72 MNm, ϕ = 0.9, M_n = 2.1 MNm, and M_{ult} = 1.89 MNm

3.4 MODELLING STRUCTURE NONLINEARITY

As mentioned earlier, the analysis of piles with structural nonlinearity essentially employs the same solutions as those for a linear (elastic) pile, but with varying bending rigidity E_pI_p beyond cracking load. The analysis for an elastic pile was elaborated previously (Guo, 2006), and recaptured in Table 4. As shown later, the values of M_{max} gained are negligibly different between elastic pile (EI) and cracked pile, but for an extremely high EI (shown elsewhere). The new E_pI_p for each M_{max} (or load) may thus be calculated using Equation (4), together with M_{cr} from Equation (3), and $(EI)_{cr}$ (via Equation (9) from **r**ectangular **b**lock **s**tress method (RBS).

The M_{cr} and E_pI_p may be deduced using measured pile response, as with the parameters G_s and LFP for linear piles, using GASLFP. A measured M_{cr} should correspond to initial point of deviation of the predicted P_t–y_o curve (using EI) from the measured curve. Beyond the M_{cr}, the E_pI_p is adjusted to minimise the derivation between the two curves, until it reduces to the final cracked rigidity $(EI)_{cr}$ at maximum failure load. A 'measured' k_r may be deduced using Equation (3) and the measured M_{cr} (such as k_r = 16.7~62.7 mentioned earlier), and the obtained E_pI_p for various M_{max} together with M_{cr} and $(EI)_{cr}$ allow Equation (4) to be justified.

The impact of reduced rigidity (owing to cracking) on a fictitious pile response is illustrated using GSLFP prediction. The pile with d = 0.373 m, L = 15.2 m, and EI = 80.0 MNm^2 was installed in the sand having ϕ_s = 35°, γ_s' = 9.9 kN/m^3, G_s = 11.2 MPa, and ν_s = 0.3. The LFP was described by α_o= 0, n = 1.6 and $N_g = 0.55K_p^2$. Under a head load P_t of 400 kN, the predicted profiles of deflection y, bending moment M, slope θ, shear force V, and on-pile force per unit length p are illustrated in Figure 3 for EI = 80.0 MNm^2 and E_pI_p= 8.0 MNm^2. The figures indicate the reduction in rigidity leads to (1) significant increase in the pile deflection and slope (all depth), and some increases in the local maximum V and p, and in the slip depth x_p; however, (2) little alteration in the bending moment profile. The results legitimatize the back-estimation of E_pI_p using measured y_o, and the M_{max} predicted from elastic-pile in Equation (4).

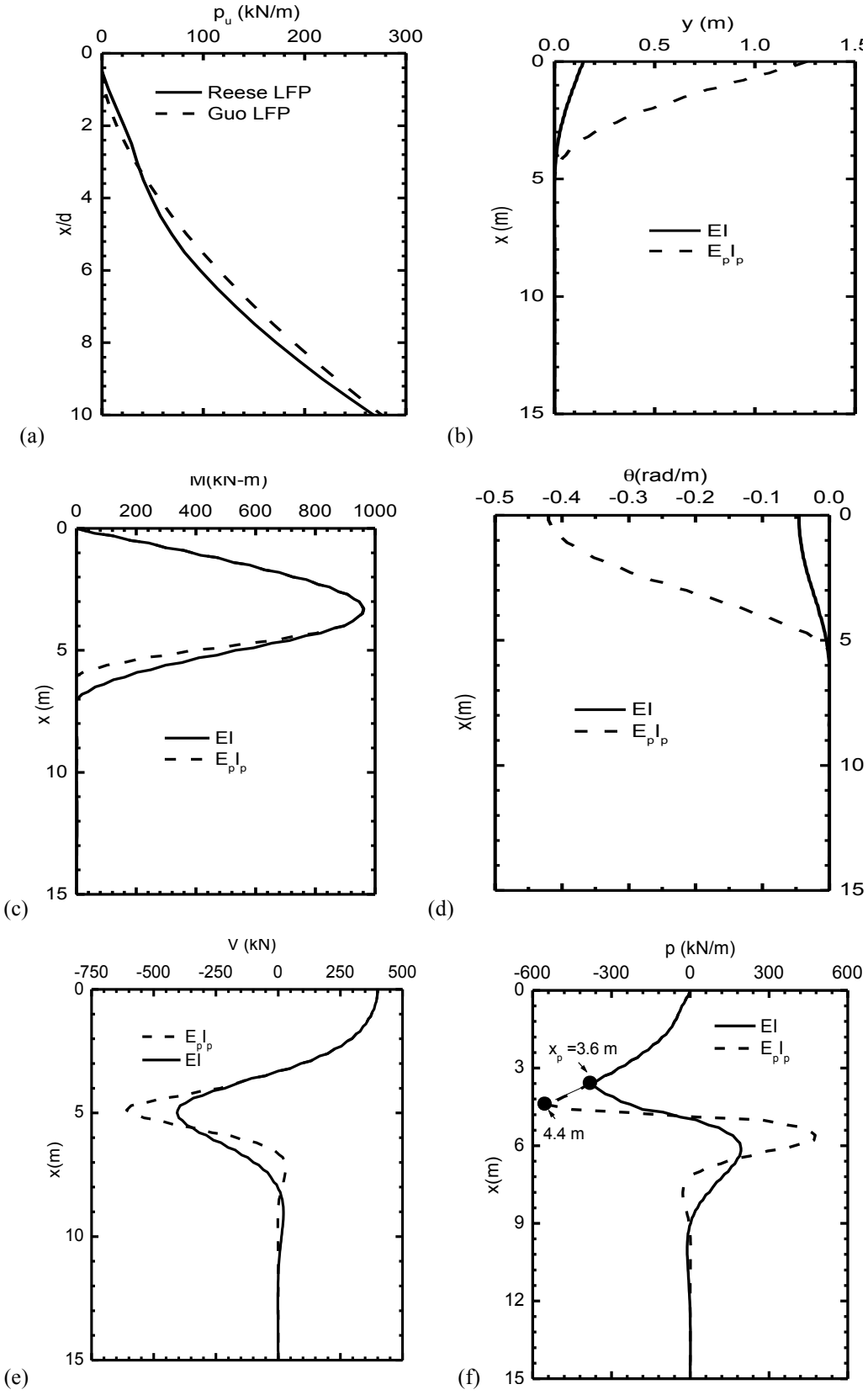

Figure 3: Effect of concrete cracking on pile response: (a) LFPs, (b) deflection (*y)* profile, (c) bending moment (*M*) profile, (d) slope (θ) profile, (e) shear force (V) profile and (f) soil reaction (*p*) profile.

Table 4: Procedure for analysis of nonlinear piles

Steps	Actions
Elastic pile	
1	Input pile properties including: d, L, E_pI_p, I_p, and e, and calculate E_p by $E_p = E_pI_p/(\pi d^4/64)$ or $= E_pI_p/(bh^3/12)$
2	Determine parameters α_s, n and N_g for LFP based on Eq. (1). For sand, average values of γ_s, ϕ are estimated over a depth of $5d$; and average shear modulus G_s over a depth of $10d$. For clay, an average value of s_u is estimated over a depth of $5d$, and shear modulus G_s are correlated to an average s_u over a depth of $10d$. For a layered soil profile with shear strength increases or decreases dramatically, n may be higher or lower than 0.7, respectively
3	Calculate critical length L_{cr}, if the value of L_{cr} < 5d for sand (or < 10d for clay), the average shear modulus is reselected to repeat the calculation of 1 and 2.
4	Compute k and N_p
Nonlinear pile	
1	Calculate the M_{max} and pile deflection y_o at each load level for elastic pile (EI)
2	Determine M_{cr} using Eq. (3)
3	Calculate the critical load P_{cr} by taking M_{max} in step 2 as the M_{cr}.
4	Compute the M_{ult} and $(EI)_{cr}$ using the **r**ectangular **b**lock **s**tress method (RBS), in terms of pile size, rebar strength and its layout, and concrete strength
5	Calculate bending rigidity E_pI_p for each load level above the P_{cr}, by substituting values of EI, $(EI)_{cr}$, M_{cr} and a series of M_{max} into Eq. (4),
6	Compute pile deflection using new E_pI_p and program GASLFP for each load.

4 ANALYSIS ON TWO NONLINEAR PILES

Investigation was conducted into four piles tested in sand and two piles in clay that manifested structure nonlinearity. Owing to space limitation, only two piles are presented herein, for which (1) shear modulus is taken as an average value over a depth of $10d$; (2) Poisson's ratio is assumed to be 0.3; and (3) γ_s and ϕ_s are taken as average values over a depth of $5d$.

4.1 A PILE TESTED IN SAND

A prestressed pile, P7 was instrumented with strain gauges and inclinometers, and tested individually under a lateral load applied near the GL (e = 0) (Huang *et al*., 2001). The soil profile at the site consisted of fine sand (SM) or silt (ML), and occasional silty clay. The ground water is located 1 m below the GL. Over a depth of 15 m, the average SPT blow count, $\overline{N}$ was 16.9; the friction angle ϕ_s was 32.6º (Teng 1962), and the effective unit weight, γ_s' was 10 kN/m^3.

The pipe pile (P7) was infilled with concrete, reinforced with 19@19 rebars, 38@9 high strength steel wires that have a concrete cover of 30 mm. It was 34.0 m long, 0.8 m O.D., and 0.56 m I.D. The strength values are (1) f_y (outer pipe pile) = 1226 MPa, f_y (infilled material) = 471 MPa, f_c' (prestressed concrete) = 78.5 MPa, and f_c' (infilled concrete) = 20.6 MPa, respectively; and (2) An equivalent yield strength of the composite cross-section of 67.74 MPa (= $(E_p/151000)^2$), as $E_p = 3.93\times10^7$ kPa determined from EI =0.79 GN-m^2. The parameters allow the following to be calculated: (1) M_{cr} = 277.4 ~ 443.9 kNm using k_r = 19.1~31.5, y_r = 0.4 m and Equation (3). And (2) M_{ult} = 1.89 MN-m, and $(EI)_{cr}/EI$ = 0.146, using the RSB method (see Table 3).

The elastic-pile analysis was based on (1) n = 1.7, α_s= 0 and $N_g = 1.0K_p^2$ = 11.13, as deduced from the DMT tests shown in Figure 4 (Huang *et al*., 2001), and (2) G_s = 10.8 MPa (= $0.64N$) (Guo 2006). The predicted deflection y_o is illustrated in Figure 4(b), which agrees with the measured data until P_t of 284 kN, at which M_{cr} = 464.7 kNm. This prediction provides (1) A slightly higher k_r of 33.0; and (2) A M_{ult} of 1.82 ~ 2.0 MN-m (as indicated by sharp increase in the measured y_o in Figure. 4(b) at P_t = 804 kN to 863 kN, which agrees well with 1.89 MN-m gained using the RBS method.

Table 5 Analysis of Pile P7 using elastic pile, and deduced E_pI_p

P_t (kN)	Measured y_o (mm)	Using elastic-pile EI			E_pI_p/EI	Using cracked E_pI_p		
		M_{max} (kNm)	y_o (mm)	x_p/d		M_{max} (kNm)	y_o (mm)	x_p/d
284	11.6	464.7	10.5	1.85	1	464.7	10.5	1.85
361	21.8	631.4	14.5	2.13	0.486	619.4	21.4	2.37
498	46.8	959.9	23.1	2.56	0.243	937.4	56.3	3.10
566	60.6	1138.0	28.0	2.75	0.204	1118.2	79.7	3.39
666	88.9	1411.8	35.8	3.02	0.176	1396.1	118.8	3.75
732	106.0	1603.5	41.4	3.18	0.167	1590.2	147.6	3.97
804	171.8	1818.0	47.9	3.35	0.160	1807.2	180.8	4.18
826.2	218.2	1886.0	50.0	3.40	0.159	1875.9	191.6	4.24

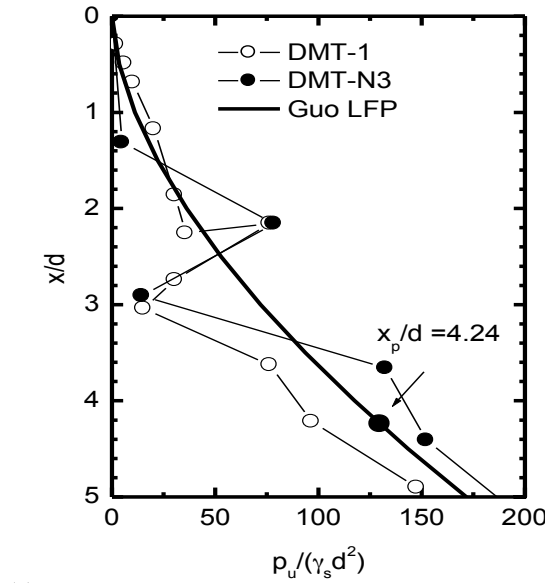

(a)

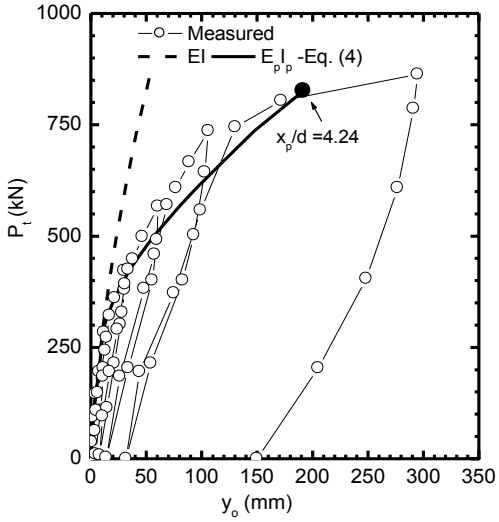

(b)

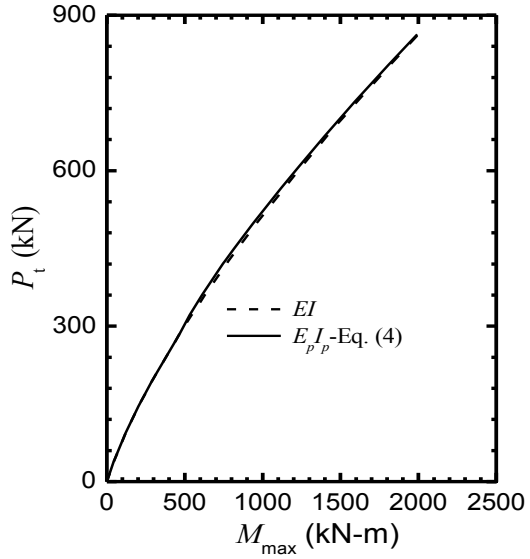

(c)

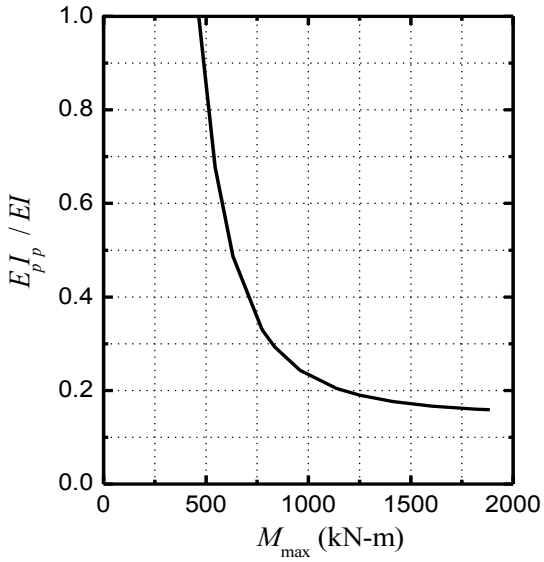

(d)

Figure 4: Comparison between measured (Huang *et al*., 2001) and predicted response of pile P7: (a) LFPs, (b) P_t-y_o curves, (3) P_t~M_{max} curves, and (4) E_pI_p/EI ~ M_{max}.

With $(EI)_{cr}$ of 0.1152 GN-m^2 (as per RSB method), M_{cr} of 464.7 kNm, and M_{ult} of 1.89 MN-m (an average of 1.82~2.0 MN-m), the E_pI_p was estimated using Equation (4) for each M_{max} (gained using EI). This E_pI_p allows new y_o and M_{max} to be estimated, which are presented in Figures 4(b) and 4(c), respectively. The measured deflection was overestimated by ~28%, indicating the accuracy of the estimated $(EI)_{cr}$ and Equation (4).

4.2 A PILE TESTED IN CLAY

Pile D was tested at a site (Nakai and Kishida 1982) with an undrained shear strength s_u = 35+0.75x (kPa, x in m < 20 m), and an average $\bar{s}_u$ over 15.48 m (= 10d) of 43 kPa. The lateral load was applied at 0.5 m above the GL. The pile had L = 30 m, d = 1.548 m, EI = 16.68 GN-m^2, E_p = 5.92×10^7 kPa, and f_c' = 153.7 MPa [≈ $(E_p/151000)^2$]. The M_{cr} was estimated as 2.81~ 4.50 MN-m (using k_r = 19.7~31.5, y_r = 0.774 m and Equation (3), which exceeds 1.33 MNm by 2.0~3.4 times. The ultimate bending moment M_{ult} was not estimated, without the reinforcement information.

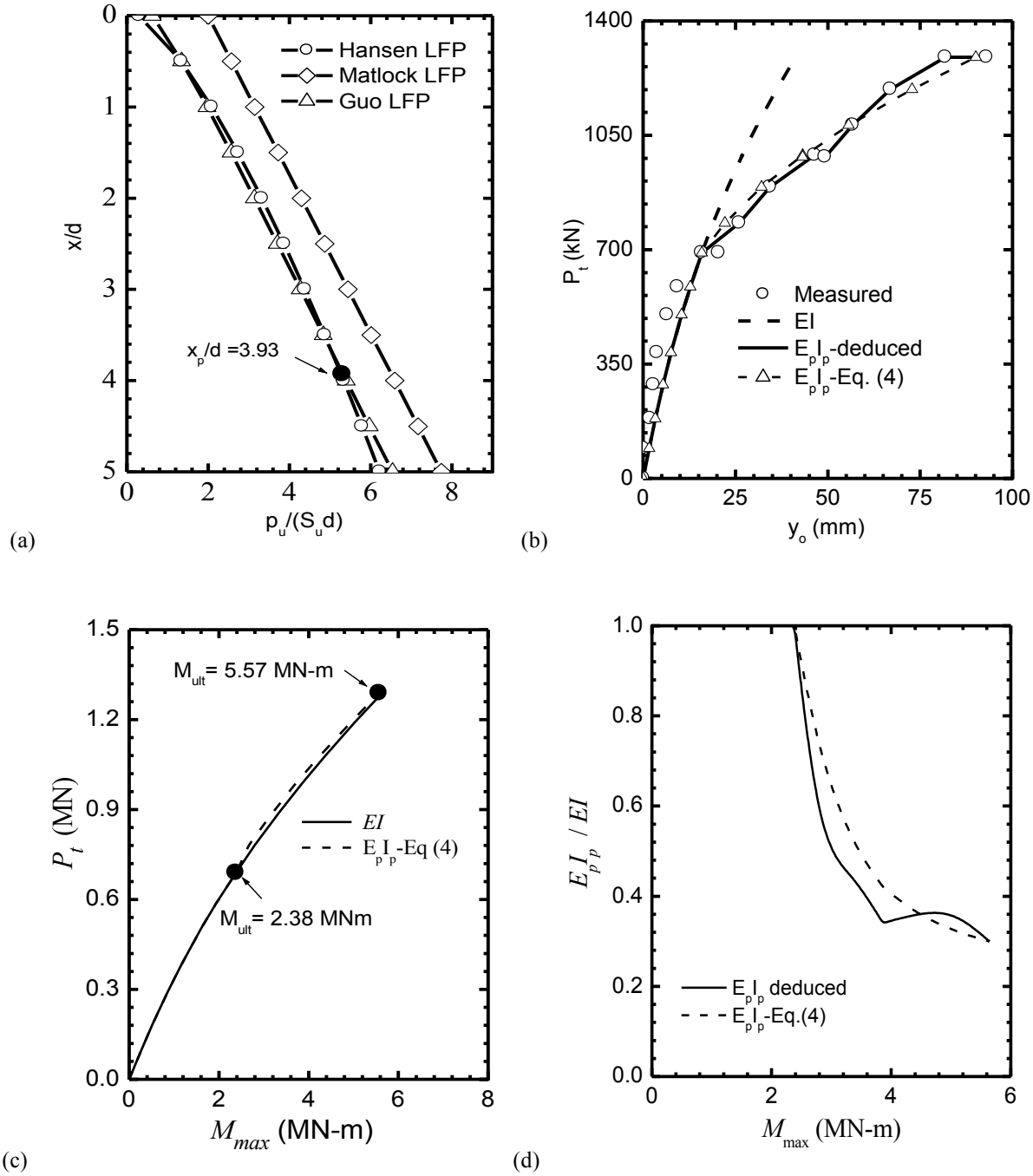

Figure 5: Comparison between calculated and measured (Nakai & Kishida, 1982) response of Pile D: (a) LFPs, (b) P_t-y_o curves, (c) P_t~M_{max} curves, and (d) E_pI_p/EI ~ M_{max}.

The elastic pile reaction was simulated using n = 0.7, α_o= 0.1 and N_g = 2.0 (see LFP in Figure 5a), and k = 3.13G_s with G_s = 5.62 MPa (=130.8s_u) (Kishida and Nakai 1977). In particular, Figure 5(a) demonstrates that the LFP within 5d is close to Hansen's LFP gained using c = 8 kPa, ϕ_s = 10°, but is far below the Matlock's LFP. The predicted pile deflection compares well with the observed one until P_t of 690 kN (see Figure 5b). The cracking M_{cr} (M_{max} at P_t = 690 kN) was deduced as 2.38 MN-m, and k_r as 16.7 using a higher E_c (= E_p) rather than the concrete modulus.

The E_pI_p was deduced using the measured deflection y_o (see Figure 5b), which in turn offers the bending moment M_{max}, as plotted in Figure 5(c). For instance, the maximum load P_t of 1289 kN incurs E_pI_p = 5.0 GN-m^2 (= 0.3EI), y_o = 90.1 mm, M_{max} = 5.57 MNm, and x_p = 6.09 m (= 3.93d). The evolution of cracking renders y_o increase by 118.2%, M_{max} reduce by 1.24%, and x_p increase by 29.3%, which resemble those noted for piles in sand (not shown herein).

Using M_{max} and E_pI_p at P_t = 1289kN, $(EI)_{cr}$ was calculated to be 4.01 GN-m^2 using Equation (4), and $(EI)_{cr}/EI$ = 0.241. Substituting $(EI)_{cr}$ and M_{max} into Eq. (4), E_pI_p was calculated, which in turn allows the deflection y_o to be computed. This deflection designated as 'E_pI_p–Equation (4)' compares well with measured one (see Figure 5b). Equation (4) is validated for this case.

5 CONCLUSIONS

A semi-empirical approach is established to capture pile response owing to structural nonlinearity. Expressions were provided for gaining cracking moment M_{cr}, flexural rigidity of cracked cross section E_pI_p, and ultimate bending moment M_{ult}. Against measured response of two laterally loaded single piles, back-estimation indicates that (1) the parameters for elastic piles are quite consistent with the previous findings by Guo (2006). (2) The proposed M_{cr}, E_pI_p and M_{ult} provide good prediction of the pile response against measured data and (3) the modulus of rupture k_r of 16.7 (clay) and 33.0 (sand) are close to those adopted for structural beams, although a very high k_r of 62.7 (thus resulting in higher M_{cr}) for a pile in sand was deduced (shown elsewhere). The use of the k_r for beams would render pile deflections of the later pile to be significantly overestimated. The conclusions may be incorporated into design of laterally loaded piles.

6 REFERENCES

ACI. (1993). Bridges, substructures, sanitary, and other special structures-structural properties. *ACI Manual of Concrete Practice 1993, Part 4*. Detroit.

Barton, Y. O. (1982). Laterally loaded model piles in sand: Centrifuge tests and finite element analysis, University of Cambridge. **Ph. D Thesis**.

Brinch Hansen, J. (1961). The ultimate resistance of rigid piles against transveral forces. Copenhagen, Denmark, The Danish Geotechnical Institute Bulletin No. 12.

Broms, B. B. (1964). "Lateral resistance of piles in cohesionless soils." *Journal of Soil Mechanics and Foundation Engineering Division, American Society of Civil Engineers* **90**(3), 123-156.

BSI (1985). Structural use of concrete. *BS 8110, London, Parts 1–3*.

Chiou, J.-S., H.-H. Yang and C.-H. Chen (2009). "Use of plastic hinge model in nonlinear pushover analysis of a pile." *Journal of Geotechnical and Geoenvironmental Engineering, ASCE* **135**(9), 1341-1346.

EC2 (1992). Design of concrete structures—Part 1-1 General rules and rules for buildings. *ENV 1992-1-1*. Brussels, Belgium.

Guo, W. D. (2001a). *Lateral pile response due to interface yielding*. Proceedings of 8th International Conference Civil and Structural Engineering Computing, CIVIL-COMP2001, paper 108, Eisenstadt, nr Vienna, Austria.

Guo, W. D. (2006). "On limiting force profile, slip depth and lateral pile response." *Computers and Geotechnics* **33**(1), 47-67.

Guo, W. D. (2008). "Laterally loaded rigid piles in cohesionless soil." *Canadian Geotechnical Journal* **45**(5), 676-697.

Guo, W. D. (2009). "Nonlinear response of laterally loaded piles and pile groups." *Int. J. Numer. and Anal. Meth. in Geomech.* **33**(7), 879-914.

Guo, W. D. and F. H. Lee (2001). "Load transfer approach for laterally loaded piles." *International Journal for Numerical and Analytical Methods in Geomechanics* **25**(11), 1101-1129.

Hansen, B. J. (1961). The ultimate resistance of rigid piles against transveral forces. Copenhagen, Denmark, The Danish Geotechnical Institute Bulletin No. 12.

Hsu, T. C. (1993). *Unified theory of reinforced concrete*. Boca Raton, Florida, USA., CRC Press, Inc. .

Huang, A. B., C. K. Hsueh, M. W. O'Neill, S. Chern and C. Chen (2001). "Effects of construction on laterally loaded pile groups." *Journal of Geotechnical and Geoenvironmental Engineering Division, ASCE* **127**(5), 385-397.

Kishida, H. and S. Nakai (1977). *Large deflection of a single pile under horizontal load*. Proceedings of 9th International conference on soil mechanics and foundation engineering, Speciality session 10, Tokyo.

Lui, E. M. (1997). *Structural steel design*. New York, CRC Press.

Matlock, H. (1970). *Correlations for design of laterally loaded piles in soft clay*. Proceedings of the 2nd offshore technology conference, Houston, Texas.

McClelland, B. and J. A. Focht (1958). "Soil modulus for laterally loaded piles." *Transactions, American Society of Civil Engineers*(Paper No. 2954), 1049-1063.

Nakai, S. and H. Kishida (1982). *Nonlinear analysis of a laterally loaded pile*. Proceedings 4th International Conference on Numerical Methods in Geomechanics, Edmonton.

Ng, C. W. W., L. Zhang and D. C. N. Nip (2001). "Response of laterally loaded large-diameter bored pile groups." *Journal of Geotechnical and Geoenvironmental Engineering Division, ASCE* **127**(8), 658-669.

Nilson, A. H., D. Darwin and C. W. Dolan (2004). *Design of concrete structures (13th Edition)*. New York, McGraw Hill.
Randolph, M. F., R. J. Jewell and H. G. Poulos (1988). *Evaluation of pile lateral load performance*. Proceedings of Engineering for Calcareous Sediments, Perth, Australia, Balkema, Rotterdam.
Reese, L. C. (1997). "Analysis of laterally loaded shafts in weak rock." *Journal of Geotechnical and Geoenvironmental Engineering Division, ASCE* **123**(11), 1010-1017.
Reese, L. C., W. R. Cox and F. D. Koop (1974). *Analysis of laterally loaded piles in sand*. Proceedings 6th Annual Offshore Technology Conference, OTC. 2080, Dallas, Texas.
Reese, L. C., W. R. Cox and F. D. Koop (1975). *Field testing and analysis of laterally loaded piles in stiff clay*. Proceedings 7th Annual Offshore Technology Conference, 2312, Dallas, Texas.
Teng, W. (1962). *Foundation Design*. N. J., Prentice Hall, Englewood Cliffs.
Whitney, C. S. (1937). "Design of reinforced concrete members under flexure or combined flexure and direct compression." *Journal of ACI* **33**, 483-498.
Zhang, L. M. (2003). "Behavior of laterally loaded large-section barrettes." *Journal of Geotechnical and Geoenvironmental Engineering Division, ASCE* **129**(7), 639-648.

APPENDIX 1 – NOTATION

The following symbols have been adopted in this paper.

a height of stress block;
A_L gradient of the LFP [FL^{-1-n}];
b width of a rectangular cross section of a pile;
c distance from extreme compression fibre to neutral axis at a section in which M_{ult} occurs;
d pile diameter;
e eccentricity of loading above groundline (GL);
E_c modulus of elasticity of concrete;
E_cI_g initial flexural rigidity of the pile;
E_p equivalent Young's modulus of pile;
f_c' characteristic value of compressive strength of the concrete;
f_c'' design value of concrete compressive strength;
f_y yield strength of reinforcement;
G^* = $(1+0.75\nu_s)$ equivalent shear modulus of soil;
G_s shear modulus of soil;
h depth of a rectangular cross section of a pile;
I_g moment of inertia of gross section of the pile;
I_e effective moment of inertia of the pile after cracking;
I_{cr} moment of inertia of cracked section;
k subgrade modulus of a spring between pile and soil;
k_1 a constant of load transfer factor;
k_r a constant for concrete rupture;
L_{cr} critical length of a pile;
M_{cr} cracking moment;
M (M_{max}) bending moment in the pile (maximum M);
M_n nominal or calculated ultimate moment;
M_t moment applied at the pile at the GL;
M_s and M_c moments about the neutral axis induced by normal stress in the rebars and concrete, respectively;
n power of the sum of α_c and x;
N blow count of Standard Penetration Tests (SPT) test;
N_g a gradient correlated compressive strength with the limiting pile – soil pressure at ground level;
N_p fictitious tension of a fictitious membrane linking the springs around the pile;
P_t lateral load applied at pile head;
P_{xs} and P_{xs} axial loads distributed on the rebars and concrete, respectively;
P_x total axial load;
p_u limiting force per unit length [FL^{-1}];
r pile radius;
s_u undrained shear strength [FL^{-2}];
V shear force in a pile;
x depth below ground level [L];
x_p slip depth;
y (y_o) pile deflection (y at ground level);
y_r distance from the centroidal axis of gross section to the extreme fibre in tension;
α_c a constant to include the force at ground level [L];
α_1 ratio of average concrete stress;
β_1 ratio of stress block depth;
ϕ ultimate moment reduction factor;
ϕ_s angle of friction of soil;
γ load transfer factor;
γ_s (γ_s') unit weight of the soil (effective γ_s);
θ the curvature.
λ reciprocal of characteristic length of the pile;
σ_{si}, σ_c normal stress in the rebars and concrete, respectively;
ν_s Poisson's ratio of soil;.